

Synthesis of a Nanosized Carbon-Supported Ni Composite and Its Remarkable Catalysis for Hydrogen Desorption from the LiBH₄–2LiNH₂ System

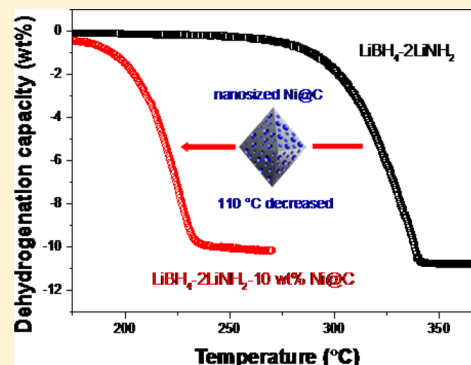
Yi Zhang,[†] Yongfeng Liu,^{*,†,‡} Xin Zhang,[†] You Li,[†] Mingxia Gao,[†] and Hongge Pan[†]

[†]State Key Laboratory of Silicon Materials, Key Laboratory of Advanced Materials and Applications for Batteries of Zhejiang Province & School of Materials Science and Engineering, Zhejiang University, Hangzhou 310027, China

[‡]Key Laboratory of Advanced Energy Materials Chemistry (Ministry of Education), Nankai University, Tianjin 300071, China

S Supporting Information

ABSTRACT: A nanosized Ni@C composite (Ni particles: < 10 nm) was successfully synthesized by casting a Ni-based metal–organic framework MOF-74(Ni) filled with furfuryl alcohol at 700 °C. The resulting Ni@C composite exhibits remarkable catalytic activity for reducing the operating temperature of hydrogen release from the LiBH₄–2LiNH₂ system. The LiBH₄–2LiNH₂–10 wt % Ni@C sample releases approximately 10 wt % of hydrogen at 135–250 °C, and the end temperature for hydrogen release is reduced by 110 °C in comparison to that of the pristine sample. During dehydrogenation, nanosized Ni remains almost unchanged and only works as a catalyst to reduce kinetic barriers of hydrogen release from the LiBH₄–2LiNH₂ system, which is responsible for lowered dehydrogenation temperatures of the Ni@C-containing sample. More importantly, the dehydrogenated Ni@C-containing sample presents a loose porous morphology that slightly improves its rehydrogenation properties.



1. INTRODUCTION

Hydrogen represents one of the most promising alternatives to fossil fuels in terms of future energy systems when considering issues of renewability, efficiency, ecosystem sustainability, and natural energy resource supply.^{1–3} Tremendous efforts have been devoted to developing a safe, efficient, and economic hydrogen storage system over the past decades.^{4–8} Solid-state complex hydrides such as metal borohydrides, alanates, and amides/imides are regarded as the most promising candidates for hydrogen storage due to their high gravimetric and volumetric hydrogen densities.^{9–15} However, practical applications of these lightweight hydrides are still restricted by their problematic thermodynamic and kinetic properties. Numerous studies have been conducted to improve hydrogen storage properties of metal complex hydrides.^{16–24} It has been proven that creating a local combination of hydridic (H[−]) (Lewis base) and protic (H⁺) atoms (Lewis acid) effectively lowers dehydrogenation/hydrogenation temperatures.^{25,26} For instance, metal amide–hydride combinations, amidoboranes, and borohydride ammoniates exhibit significantly lower dehydrogenation temperatures than their counterparts.^{12–14,27–35}

In 2005, Pinkerton et al. presented a novel LiBH₄–2LiNH₂ combination system that releases all available hydrogen in LiBH₄ and LiNH₂.²⁷ It was observed that more than 10 wt % of hydrogen is released from this novel combination system within a temperature range of 250–350 °C, which is distinctly superior

to individual constituents alone under the same conditions.^{10,12}

Subsequently, Meisner et al. described the compositional dependence of decomposition behaviors of (LiNH₂)_x(LiBH₄)_{1-x} composites.³⁶ Their results showed that the LiBH₄–2LiNH₂ system should offer the optimal combination of maximized hydrogen desorption capacity and minimal ammonia generation due to the presence of equivalent H[−] and H⁺ in this system. Unfortunately, the dehydrogenation temperature of the LiBH₄–2LiNH₂ system remains high for practical applications. Moreover, hydrogen desorption is of exothermic nature, which, in association with the emission of NH₃ byproducts, also limits its practical applications, especially for mobile applications.

One means of reducing dehydrogenation temperatures and improving LiBH₄–2LiNH₂ system performance levels involves introducing high-efficiency catalysts such as transition metals and their chlorides and oxides.^{37–42} In 2006, Pinkerton et al. first explored the effects of Pd, Pt, PdCl₂, PtCl₂, and Pt/Vulcan carbon on the hydrogen release of LiB_{0.33}N_{0.67}H_{2.67},³⁷ which has an equivalent composition as the LiBH₄–2LiNH₂. It was found that adding 5 wt % Pd either as Pd metal particles or as PdCl₂ reduces the midpoint dehydrogenation temperature by 43 and 76 °C, respectively. Subsequently, the catalytic functions of Ni,

Received: September 22, 2015

Revised: October 11, 2015

Published: October 14, 2015



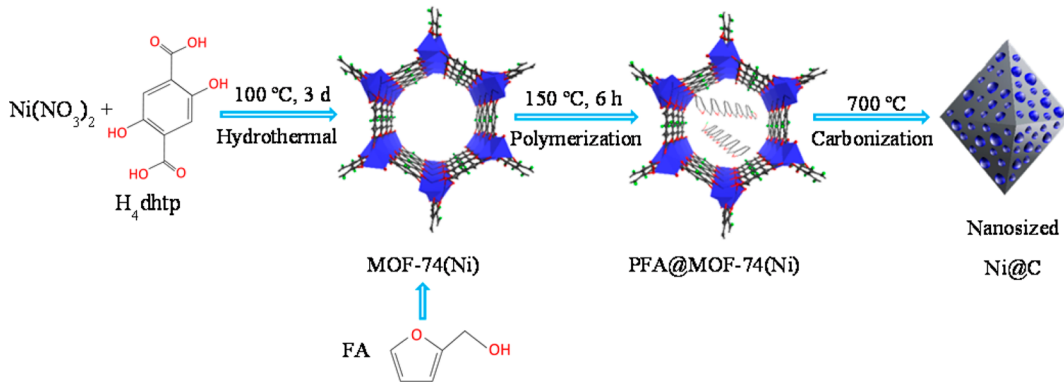


Figure 1. Schematic preparation process of the nanosized Ni@C composite.

Fe, Zn, and Co and their chlorides were examined.³⁸ It was shown that the 5 wt % NiCl_2 -added $\text{LiB}_{0.33}\text{N}_{0.67}\text{H}_{2.67}$ sample evolved roughly 10.0 wt % of hydrogen within a temperature range of $180\text{--}250^\circ\text{C}$, a value nearly 100°C lower than that of the pristine sample. Moreover, Tang et al. found considerably superior effects of CoCl_2 over NiCl_2 , with the 5 wt % CoCl_2 -added $\text{LiBH}_4\text{--}2\text{LiNH}_2$ system releasing more than 8 wt % of hydrogen at the low temperature of 155°C .³⁹ Our recent results also indicated that adding a small quantity of CoO or Co_3O_4 may also significantly decrease the dehydrogenation temperature of the $\text{LiBH}_4\text{--}2\text{LiNH}_2$ system.^{41,42} The $\text{LiBH}_4\text{--}2\text{LiNH}_2\text{--}0.05/3\text{Co}_3\text{O}_4$ composite desorbed approximately 9.9 wt % through a four-step reaction and caused a 96°C reduction in midpoint temperature levels in comparison to the additive-free sample.⁴¹ More importantly, the first and third steps of the $\text{LiBH}_4\text{--}2\text{LiNH}_2\text{--}0.05/3\text{Co}_3\text{O}_4$ composite dehydrogenation were endothermic, differing considerably from the additive-free sample process. More specifically, the dehydrogenated Co_3O_4 -containing system absorbed approximately 1.7 wt % of hydrogen under 110 bar hydrogen at 220°C . A similar phenomenon was found in the CoO -added system.⁴² Mechanistic analyses revealed that during thermal dehydrogenation transition-metal-based catalysts undergo a chemical reduction process to ultimately convert into metal nanoparticles. In-situ formed transition metal nanoparticles were finely dispersed across samples and were used as the active catalytic species for improving thermodynamic and kinetic properties of dehydrogenation reactions in the $\text{LiBH}_4\text{--}2\text{LiNH}_2$ system.^{41,42} It is therefore very desirable to further improve the dehydrogenation performance of the Li–B–N–H system by directly preparing ultrafine metallic nanoparticles of high catalytic activity. More recently, we proposed a novel in situ method for the preparation of TiO_2 nanoparticles supported by carbon that uses a Ti-based metal–organic framework (MOF) as a template.²³ The synthesized ultrafine nanocrystalline $\text{TiO}_2@\text{C}$ presents superior levels of catalytic activity for hydrogen storage reactions of NaAlH_4 due to the synergistic effect of Ti-based active species and the hydrogen spillover functions of carbon. The $\text{NaAlH}_4\text{--}9$ wt % $\text{TiO}_2@\text{C}$ sample releases hydrogen from 63°C and reabsorbs from 31°C , and these values are reduced by 114 and 69°C relative to those of pristine NaAlH_4 , respectively. Such superior effects are also anticipated for other transition-metal-based catalysts in catalyzing hydrogen storage reactions of complex hydrides.

For this study, we prepared successfully metallic Ni nanoparticles supported by carbon (called Ni@C) using the same strategy reported in previous studies,^{23,43} and we

examined its catalytic effects on dehydrogenation behaviors of the $\text{LiBH}_4\text{--}2\text{LiNH}_2$ system. It was observed that doping a small quantity of nanosized Ni@C considerably decreases the dehydrogenation temperature of the $\text{LiBH}_4\text{--}2\text{LiNH}_2$ system. In comparison with the pristine sample, the onset temperature of hydrogen release from the $\text{LiBH}_4\text{--}2\text{LiNH}_2\text{--}10$ wt % Ni@C sample was lowered by 110°C , and approximately 10.0 wt % of hydrogen was released within 25 min at 220°C . The chemical state of metallic Ni upon dehydrogenation was also studied and is discussed.

2. EXPERIMENTAL SECTION

2.1. Sample Preparation. Commercially available LiBH_4 (Acros, 95%) and LiNH_2 (Alfa Aesar, 95%) were used as received without further purification. The nanosized Ni@C composite was synthesized using a metal–organic framework, MOF-74(Ni), as a template and using the furfuryl alcohol (FA, Aladdin, 98%) as a carbon precursor (Figure 1). First, the MOF-74(Ni) was synthesized following the procedure reported by Caskey et al.⁴³ In typical experiments, 4 mmol of 2,5-dihydroxyterephthalic acid (H_4dhtp , TCI, 98.0%) and 8 mmol of $\text{Ni}(\text{NO}_3)_2\cdot6\text{H}_2\text{O}$ (Aladdin, 99%) were added to a solution with 30 mL of dimethylformamide (DMF, Aladdin, 99.9%), 30 mL of ethanol, and 30 mL of water. The suspension was stirred until the solid-state reactants had completely dissolved. The solution was transferred into a 200 mL Teflon liner and was placed in a stainless steel autoclave for 3 days of heating at 100°C in an oil bath. After being cooled to room temperature, the mother liquor was filtered. The precipitate was washed twice with DMF and twice with ethanol to remove the organic residuals and DMF in sequence. The solid-state product was activated under a vacuum at 240°C for 12 h. X-ray diffraction examination results confirmed the formation of pure MOF-74(Ni) (Figure S1, Supporting Information). Subsequently, the furfuryl alcohol was introduced into pores of the framework by stirring together 15 mL of FA, 35 mL of ethanol, and 0.5 g of the activated product for 24 h under Ar atmosphere conditions at room temperature. After being carefully filtrated and washed with ethanol, the FA-filled MOF-74(Ni) composite was transferred into a tube furnace and heated at 80°C for 24 h and then at 150°C for 6 h under Ar flow to polymerize FA accommodated in the pores. Finally, the polyfurfuryl alcohol@MOF-74(Ni) composite was carbonized at 700°C to produce nanosized Ni supported by carbon (denoted as nanosized Ni@C). The C contents of the nanosized Ni@C composite were quantitatively determined based on thermogravimetric (TG) and differential scanning calorimetry (DSC) measurements

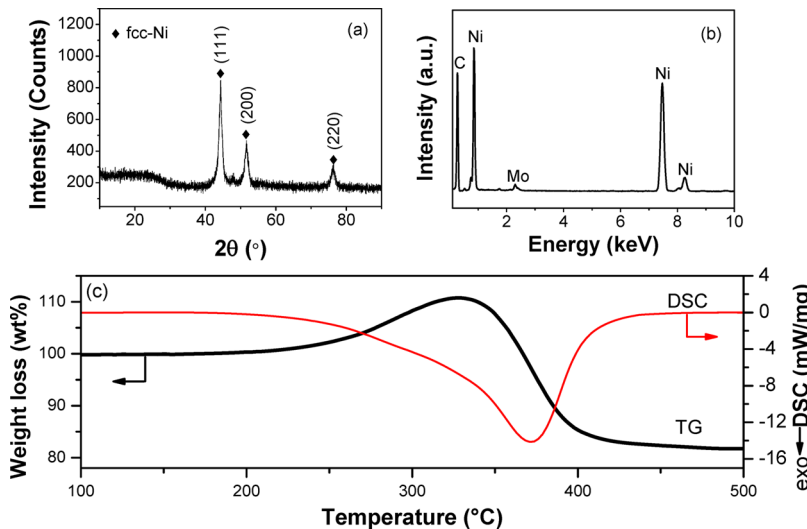


Figure 2. XRD pattern (a), EDS spectrum (b), and TG-DSC curve (c) of the calcined Ni@C composite.

performed using a NETZSCH TG 209F3 instrument under standard airflow conditions of 40 mL/min. Approximately 5 mg of the sample was heated in an Al_2O_3 crucible from 50 to 500 °C at a rate of 5 °C/min. The resulting nanosized Ni@C was introduced into the LiBH_4 – 2LiNH_2 system, and eight samples with a composition of LiBH_4 – 2LiNH_2 – $x\text{Ni@C}$, where $x = 0, 0.05, 0.3, 0.8, 3, 5, 10$, and 15 wt %, were prepared by ball milling corresponding materials on a planetary ball mill (QM-3SP4, Nanjing) at 500 rpm for 24 h. The ball-to-sample weight ratio was approximately 120:1. The milling process was carried out through alternating 12 min milling periods and 6 min rest periods to minimize the temperature increment of the samples. All of the samples were handled in a glovebox (MBRAUN 200B, Germany) filled with high purity Ar ($\text{H}_2\text{O} < 1 \text{ ppm}$; $\text{O}_2 < 1 \text{ ppm}$) to prevent moisture and oxygen contamination.

2.2. Property Evaluations. Temperature-dependent decomposition behaviors were measured using a homemade temperature-programmed-desorption (TPD) system coupled with a mass spectrometer (Hiden QIC-20, England) for monitoring gaseous compositions produced from the sample upon heating. Approximately 20 mg of the sample was loaded into the TPD-MS measurement system and then heated from room temperature to 400 °C at a rate of 2 °C/min under an Ar flow pace of 20 mL/min. Quantitative evaluations of hydrogen desorption/absorption were performed using a homemade Sievert-type apparatus. On average, 100 mg of sample was used and gradually heated from ambient temperatures to the desired temperature at a rate of 2 °C/min under static vacuum conditions for dehydrogenation and at 1 °C/min under 100 bar of initial hydrogen pressure for hydrogenation. For the isothermal examinations, the samples were rapidly heated to a preset temperature and then held at this temperature throughout the measurement period. Heat effects of the LiBH_4 – 2LiNH_2 composites with and without Ni@C were examined under Ar atmosphere conditions via differential scanning calorimetry (DSC) on a NETZSCH DSC 200F3 unit installed in an argon-filled glovebox. Approximately 2 mg of sample was used each time and was heated in an Al crucible from 50 to 400 °C at a ramping rate of 5 °C/min.

2.3. Structural and Morphological Characterization. Sample phase structures were characterized via powder X-ray diffraction (XRD) on a PANalytical X'Pert diffractometer

equipped with Cu K α radiation (40 kV and 40 mA). Data were collected from 10 to 90° (2θ) with a step increment of 0.05° at ambient temperatures. The powder samples were sealed in a specially designed container with Scotch tape to prevent oxygen and moisture contamination. N–H and B–H vibrations in the Li–B–N–H composites were identified using a Bruker Tensor 27 Fourier transform infrared spectrometer (FTIR, Germany) with a resolution of 4 cm $^{-1}$. All of the powder samples were first evenly mixed with potassium bromide (KBr) in a weight ratio of 1:150 and then cold-pressed to form pellets with a diameter of 13 mm and a thickness of 0.5 mm. The transmission mode was adopted, and each spectrum was obtained after 16 scans. The sample morphologies were observed via scanning electron microscopy (SEM, Hitachi, S-4800) and transmission electron microscopy (TEM, FEI, Tecnai G2 F20 S-TWIN). The chemical composition of the nanosized Ni@C composite was analyzed using an energy-dispersive X-ray spectrometer (EDS) attached to an FEI Tecnai G2 F20 S-TWIN transmission electron microscope. The distribution of elemental Ni in the dehydrogenated sample was observed using an aberration-corrected high-angle annular dark field scanning transmission electron microscope (HAADF-STEM, Titan ChemiSTEM, 200 kV). The chemical state of Ni was identified using a parallel-equipped electron energy loss spectroscopy (EELS, Gatan, Pleasanton, CA) detection system. The spectrum was acquired at a Ni L_{2,3}-edge, and the full width at the half-maximum (fwhm) point of the zero-loss peak spanned approximately 1.5 eV.

3. RESULTS AND DISCUSSION

3.1. Structure and Morphology of the Prepared Samples. The Ni-based catalyst was synthesized by heating the FA-filled MOF-74(Ni) at 700 °C. Figure 2(a) shows the XRD pattern of the resulting product. Only three diffraction peaks were detected at 44.3, 51.7, and 76.2° (2θ), which correspond to characteristic reflections of metallic Ni in the fcc structure. The low intensities of reflections associated with broad widths suggest the presence of poor crystallization processes and/or small particle/grain sizes. Moreover, the relatively high background denotes the existence of amorphous species. The EDS examination results show that in addition to Ni the resulting product should be composed of C, as shown in

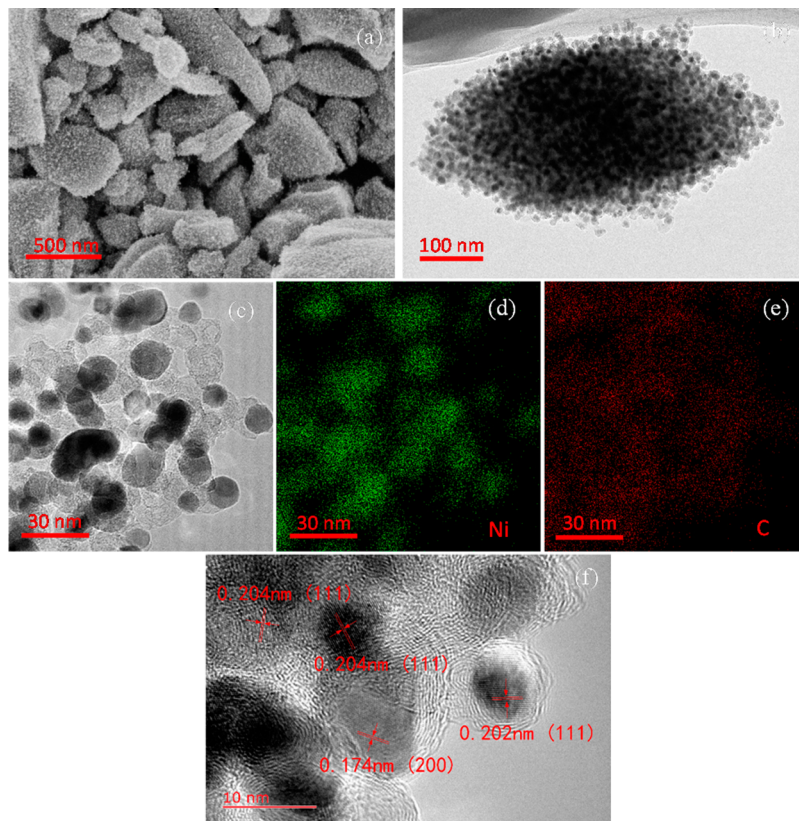


Figure 3. SEM image (a), TEM and enlarged images (b,c), EDS mapping (d,e), and HRTEM image (f) of the prepared Ni@C composite.

Figure 2(b). Here, it should be noted that the Mo signal can be attributed to the Mo mesh used in this experiment. Additional TG-DSC measurements (Figure 2(c)) showed that the total weight loss was 18.3 wt % when the as-prepared sample was heated from room temperature to 500 °C under air atmosphere. XRD examination revealed that the resulting product collected after TG-DSC experiment was mainly composed of NiO (Figure S2, Supporting Information). Thus, the concentrations of Ni and C can be calculated by the following equations

$$x_{\text{Ni}} \cdot \frac{M_{\text{NiO}}}{M_{\text{Ni}}} = 1 - W_{\text{Loss}} \quad (1)$$

$$x_{\text{C}} = 1 - x_{\text{Ni}} \quad (2)$$

where x_{Ni} and x_{C} are the concentrations of Ni and C, respectively; M_{NiO} and M_{Ni} are the relative molecular weight of NiO and Ni, respectively; and W_{Loss} is the total weight loss measured by TG. As a result, the concentrations of Ni and C were measured at approximately 64.2 and 35.8 wt %, respectively.

Figure 3(a) presents an SEM image of the synthesized sample. It is evident that the 700 °C calcined sample presented very irregular shapes with sizes ranging from 0.2 to 1 μm. TEM observation on a representative particle displayed numerous small particles inlaid along the matrix surface (Figure 3(b,c)). Further EDS analysis revealed that these small particles were Ni particles, and the gray matrix was likely carbon material (Figure 3(d,e)). High-resolution TEM (HRTEM) images shown in Figure 3(f) clearly indicated the (111) and (200) planes of the fcc-Ni, serving as additional evidence for the existence of metallic Ni. More importantly, particle sizes of metallic Ni were

less than 30 nm in diameter (Figure 3(c, f)). We therefore believe that the 700 °C calcined product is composed of crystalline Ni nanoparticles supported by carbon, which we hereinafter refer to as nanosized Ni@C composite.

To evaluate the catalytic function of the prepared nanosized Ni@C composite, the composite was introduced into the LiBH₄-2LiNH₂ system via ball milling, and dehydrogenation/hydrogenation behaviors of the resulting samples were systematically studied. Eight samples with compositions of LiBH₄-2LiNH₂- x Ni@C ($x = 0, 0.05, 0.3, 0.8, 3, 5, 10, 15$ wt %) were prepared. Figure 4 shows the XRD patterns of the milled LiBH₄-2LiNH₂- x Ni@C samples. It is evident that the pristine LiBH₄-2LiNH₂ sample was mainly composed of α -Li₄BN₃H₁₀ as the primary phase and β -Li₂BNH₆ as the minor phase, indicating that a chemical reaction occurred between LiBH₄ and LiNH₂ during the ball milling process, producing the new quaternary Li-B-N-H compounds. This result is in excellent consistence with previous reports.^{27,36} For the nanosized Ni@C-added samples, the α -Li₄BN₃H₁₀ phase still dominated the XRD profiles, and the reflections of β -Li₂BNH₆ were nearly undetectable.⁴⁴⁻⁴⁶ With increasing levels of Ni@C, peak intensities of the α -Li₄BN₃H₁₀ phase decreased gradually due to dilution effects. When $x > 3$ wt % in LiBH₄-2LiNH₂- x Ni@C, the strongest reflection of metallic Ni was also detected, and this gradually intensified.

3.2. Catalytic Effects of Nanosized Ni@C in the LiBH₄-2LiNH₂- x Ni@C System. Figure 5 shows the TPD-MS curves of the LiBH₄-2LiNH₂- x Ni@C ($x = 0, 0.05, 0.3, 0.8, 3, 5, 10, 15$ wt %) samples as a function of temperature. For the pristine sample, a distinct hydrogen desorption peak that ranged from 260 to 350 °C and that centered at 335 °C was observed when it was heated from room temperature to 400 °C, echoing the

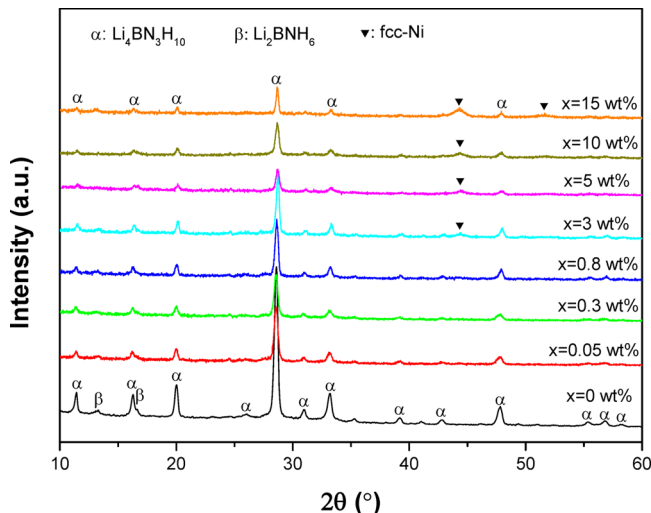


Figure 4. XRD patterns of the milled $\text{LiBH}_4\text{--}2\text{LiNH}_2\text{--}x\text{Ni@C}$ composites.

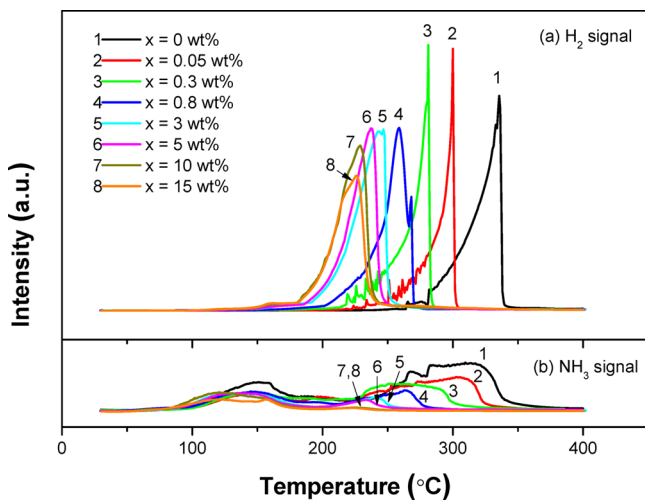


Figure 5. MS- H_2 (a) and NH_3 signals (b) of the milled $\text{LiBH}_4\text{--}2\text{LiNH}_2\text{--}x\text{Ni@C}$ composites as a function of temperature.

findings of previous reports.^{40–42} After 0.05 wt % of Ni@C was added, the dehydrogenation peak temperature declined to 300 °C, which is 35 °C lower than that of the pristine sample. As expected, an additional dehydrogenation temperature decline was obtained by adding more of the nanosized Ni@C composite. The onset temperature of hydrogen release from the $\text{LiBH}_4\text{--}2\text{LiNH}_2\text{--}10$ wt % Ni@C sample was decreased to 150 °C, representing a roughly 110 °C reduction in comparison to the pristine sample. Moreover, the dehydrogenation peak appeared at 228 °C, and most dehydrogenation processes occurred at below 250 °C. However, increasing the addition volume to 15 wt % did not decrease dehydrogenation temperatures further in combination with slightly decreased peak intensity levels. Also important to note is that the presence of nanosized Ni@C dramatically suppressed the evolution of NH_3 byproducts, and especially within the temperature range of 200–400 °C, as shown in Figure 5(b). These results suggest that adding a small amount of nanosized Ni@C can significantly reduce dehydrogenation temperatures while effectively increasing the purity of hydrogen released from the $\text{LiBH}_4\text{--}2\text{LiNH}_2$ system.

A quantitative evaluation of dehydrogenation behaviors of the $\text{LiBH}_4\text{--}2\text{LiNH}_2\text{--}x\text{Ni@C}$ samples was then conducted via volumetric release. As shown in Figure 6(a), the addition of

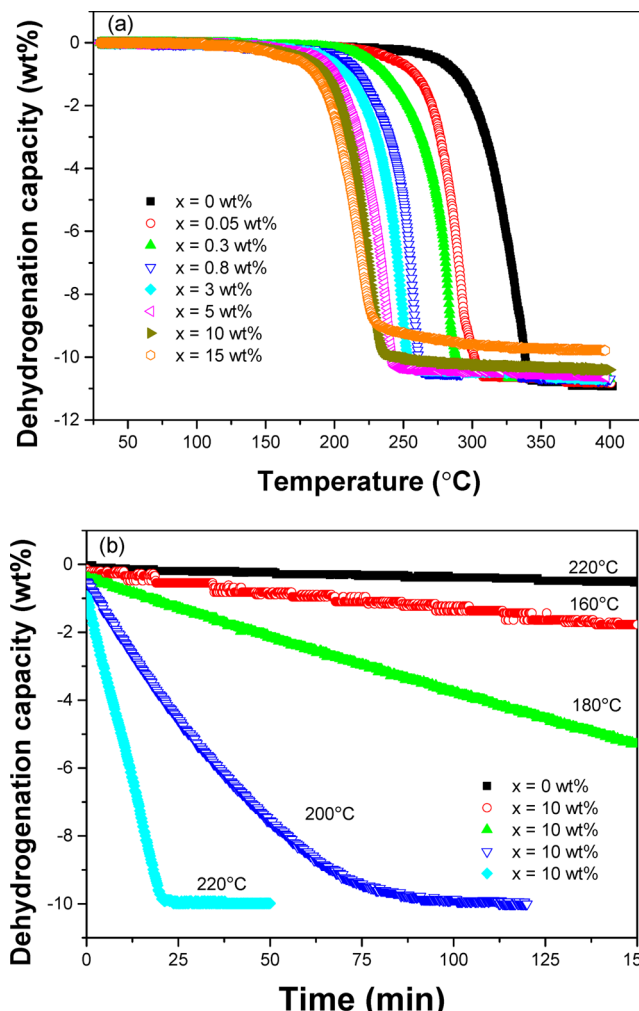


Figure 6. Nonisothermal (a) and isothermal (b) dehydrogenation curves of the milled $\text{LiBH}_4\text{--}2\text{LiNH}_2\text{--}x\text{Ni@C}$ composites.

nanosized Ni@C significantly reduced the operating temperature of hydrogen release from the $\text{LiBH}_4\text{--}2\text{LiNH}_2$ system, and this result is in good agreement with the TPD-MS results. For the pristine $\text{LiBH}_4\text{--}2\text{LiNH}_2$ sample, approximately 10.8 wt % of hydrogen was released through a one-step reaction within a temperature range of 250–345 °C. Given the presence of 0.05 wt % Ni@C, the onset dehydrogenation temperature was decreased to 200 °C, and the midpoint temperature, which corresponds to half of the dehydrogenation capacity, was reduced by 36 °C from 322 to 286 °C. After being heated to 310 °C, 10.6 wt % of hydrogen was released. While the amount of nanosized Ni@C added increased from 0.05 wt % to 10 wt %, the end temperature for the majority of hydrogen release was decreased continuously from 310 to 250 °C. However, the dehydrogenation capacity was only reduced slightly from 10.6 wt % to 10.0 wt %. This is reasonably attributed to the effective suppression of NH_3 byproduct evolution in the presence of nanosized Ni@C (Figure 5(b)), which is likely to be converted to hydrogen. Thus, approximately 10.0 wt % of hydrogen, representing 96% of the theoretical hydrogen capacity, was released from the $\text{LiBH}_4\text{--}2\text{LiNH}_2\text{--}10$ wt % Ni@C sample

within a temperature range of 135–250 °C, which is superior to any known Ni-doped Li–B–N–H system.³⁸ When nanosized Ni@C additions were further increased to 15 wt %, no appreciable decrease in dehydrogenation temperatures was observed, though the dehydrogenation capacity was held at 9 wt % when heated to 250 °C. On the basis of the above discussion, we conclude that 10 wt % Ni@C served as an optimal addition for catalyzing hydrogen desorption from the LiBH₄–2LiNH₂ system in the present study.

Figure 6(b) presents isothermal dehydrogenation curves of the LiBH₄–2LiNH₂ and LiBH₄–2LiNH₂–10 wt % Ni@C samples. It is evident that remarkable improvements in dehydrogenation kinetics were achieved by adding Ni@C, especially at low temperatures. As shown, 1.8 wt % of hydrogen was released from the 10 wt % Ni@C-containing sample within 150 min at 160 °C. This increased to 5.0 wt % of hydrogen, constituting half of the total dehydrogenation amount, while dwelling at 180 °C for 150 min. Further elevating the operating temperature accelerated the dehydrogenation reaction, releasing 10.0 wt % of hydrogen within 100 min at 200 °C and within 22 min at 220 °C. In contrast, only 0.5 wt % of hydrogen was released from the pristine LiBH₄–2LiNH₂ sample within 150 min at 220 °C.

3.3. Dehydrogenation Thermodynamics and Kinetics of Samples with and without Ni@C. To determine the source of reduced dehydrogenation temperatures and improved dehydrogenation rates found for the Ni@C-containing sample, thermodynamic and kinetic properties of the hydrogen desorption reaction of the LiBH₄–2LiNH₂ and LiBH₄–2LiNH₂–10 wt % Ni@C samples were evaluated and compared. The apparent activation energy level was quantitatively determined using Kissinger's method as follows⁴⁷

$$\frac{d \ln\left(\frac{\beta}{T_m^2}\right)}{d\left(\frac{1}{T_m}\right)} = -\frac{E_a}{R} \quad (3)$$

where E_a is the apparent activation energy level for kJ/mol; β is the heating rate for K/min; T_m is the desorption peak temperature of K; and R is the gas constant. T_m values were obtained from the TPD curves collected at heating rates of 2, 3, 4, and 5 K/min. As shown in Figure 7(a), the apparent

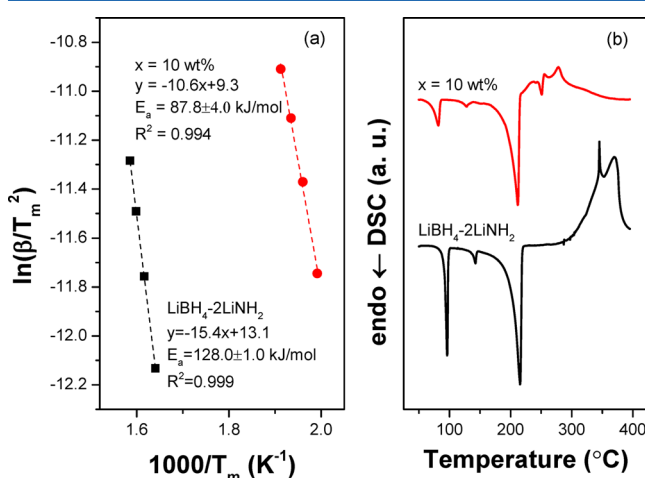


Figure 7. Kissinger plots (a) and DSC curves (b) of the LiBH₄–2LiNH₂ and LiBH₄–2LiNH₂–10 wt % Ni@C composites.

activation energy level of the pristine LiBH₄–2LiNH₂ sample was calculated at 128.0 ± 1.0 kJ/mol, which is consistent with the previous report.²² For the LiBH₄–2LiNH₂–10 wt % Ni@C sample, the E_a value was decreased to 87.8 ± 4.0 kJ/mol, representing an approximately 30% reduction for the additive-free sample. This serves as one important cause of decreased operating temperatures for hydrogen desorption from the Ni@C-containing sample.

Figure 7(b) presents the DSC curves of the LiBH₄–2LiNH₂ and LiBH₄–2LiNH₂–10 wt % Ni@C samples. Three endothermic peaks centered at 96, 143, and 215 °C and a broad exothermic peak at 270–400 °C were found in the DSC curve of the pristine LiBH₄–2LiNH₂ sample, which can be attributed to the melting of β -Li₂BNH₆, the initial NH₃ release, the melting of α -Li₄BN₃H₁₀, and hydrogen desorption, respectively.^{37–42} For the 10 wt % Ni@C-containing sample, three endothermic peaks moderately downshifted to 82, 128, and 212 °C. Additionally, the intensity of the first endothermic peak was greatly reduced, possibly due to the decreased β -Li₂BNH₆ phase in the sample as observed in the XRD profile (Figure 4). However, the exothermic peak corresponding with hydrogen release distinctly shifted to lower temperatures. Rather, it appeared right after the melting of α -Li₄BN₃H₁₀. Moreover, it dramatically declined, and this can be attributed to the offsetting of endothermic effects of α -Li₄BN₃H₁₀ melting. A comparison between the DSC and TPD curves shows that most of the hydrogen desorption of the LiBH₄–2LiNH₂–10 wt % Ni@C sample coincided well with the melting of the α -Li₄BN₃H₁₀ phase, as both processes occurred at 180–250 °C. This suggests an overlap between the majority of hydrogen desorption of the nanosized Ni@C-containing sample and α -Li₄BN₃H₁₀ melting. As reported previously,^{41,42} transition metal and compound catalytic capabilities for hydrogen release from the LiBH₄–2LiNH₂ system were closely related to reactant mobility levels. After melting occurred, high reactant mobility was achieved, making contact with active catalytic species much easier and consequently inducing rapid dehydrogenation at lower temperatures. Moreover, a small exothermic peak occurring at 300 °C may originate from the phase transition of the dehydrogenation product. These improved thermodynamics and kinetics are responsible for the significant reduction in dehydrogenation temperatures of the LiBH₄–2LiNH₂ system.

3.4. Dehydrogenation Mechanisms of the Ni@C-Containing LiBH₄–2LiNH₂ System. To elucidate dehydrogenation mechanisms of the nanosized Ni@C-containing system, solid-state products of the dehydrogenated LiBH₄–2LiNH₂–10 wt % Ni@C sample collected at various temperatures were subjected to XRD and FTIR analyses. As noted above, the prepared sample was mainly composed of α -Li₄BN₃H₁₀ and fcc Ni phases. While the sample was heated to 140 °C, no appreciable change was observed in the XRD profile (Figure 8(a)). Further FTIR examinations confirmed the presence of Li₄BN₃H₁₀ with typical B–H vibrations at 1082, 1122, 2222, 2287, and 2380 cm⁻¹ and with N–H vibrations at 3246, 3302, and 3379 cm⁻¹, as shown in Figure 8(b).^{41,42} A closer comparison reveals that the relative intensity of N–H decreased slightly for the prepared sample, denoting the consumption of a small amount of the NH₂ group corresponding to ammonia release trends observed in the TPD-MS experiment (Figure 5). After further heating the sample to 250 °C, typical reflections of the Li₄BN₃H₁₀ were invisible in the XRD pattern. A series of new diffraction peaks

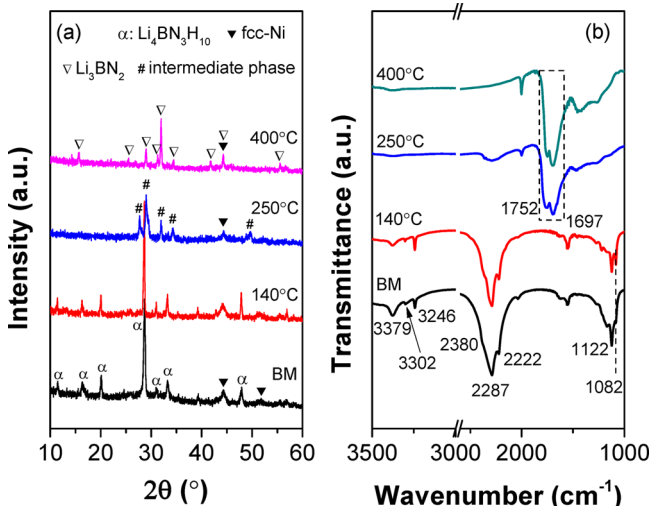
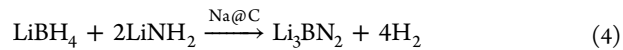


Figure 8. XRD patterns (a) and FTIR spectra (b) of the dehydrogenated LiBH₄-2LiNH₂-10 wt % Ni@C samples as a function of temperature.

were identified at 27.7, 29.0, 32.0, 34.3, and 49.6° (2θ) with strong densities assigned to a hydrogen-poor intermediate phase.⁴⁸ Meanwhile, metallic Ni was also identified as a minor phase, although its diffraction peak was weak. FTIR analyses provided additional evidence for the consumption of B-H and N-H bonds as typical N-H vibrations in the NH₂ groups (3246, 3302, and 3379 cm⁻¹), and B-H vibrations in the BH₄ groups (1082, 1122, 2222, 2287, and 2380 cm⁻¹) disappeared. However, two new absorbances were detected at 1752 and 1697 cm⁻¹ that mainly originate from B-N vibrations in Li₃BN₂, as reported previously.^{41,42,49} These results show that the LiBH₄-2LiNH₂-10 wt % Ni@C composite released the most hydrogen within a temperature range of 140–250 °C with catalytic functions of nanosized Ni@C and conversion to the Li₃BN₂ ternary nitride. We therefore believe that nanosized Ni@C composite presence promotes hydrogen release from the LiBH₄-2LiNH₂ system and likely due to the ready combination of H⁺ in NH₂ groups and H⁻ in BH₄ groups, as proposed previously.^{41,42} Upon further elevating the operating

temperature to 400 °C, characteristic reflections of the bcc-Li₃BN₂ phase with a tetragonal *I4₁/amd* structure were identified unambiguously in the XRD pattern along with the absence of the hydrogen-poor intermediate phase. This reasonably explains the presence of a weak exothermic peak at 270–400 °C in the DSC curve (Figure 7(b)). As a result, the hydrogen release process of the nanosized Ni@C-containing LiBH₄-2LiNH₂ sample can be still summarized by the following reaction.⁴⁰



The morphologies of the dehydrogenated LiBH₄-2LiNH₂ and LiBH₄-2LiNH₂-10 wt % Ni@C samples were studied further via SEM. The results are presented in Figure 9(a) and (b). The dehydrogenated pristine sample presents solid particle morphologies with sizes ranging from 0.5 to 2 μm as shown in Figure 9(a). However, a loose carbon morphology was clearly observed in the dehydrogenated Ni@C-containing sample with enlarged particle sizes (5–10 μm) (Figure 9(b)). A closer observation of a representative particle provides much clearer evidence, as shown in Figure 9(c). The loose morphology, as extensively reported, proves highly conducive to improving dehydrogenation kinetics.^{41,42} Moreover, the dark-field HAADF-STEM image shows that numerous nanoparticles were dispersed throughout the dehydrogenated Ni@C-containing sample and were proven to be metallic Ni via EDS mapping analysis (Figure 9(d,e)). An additional EELS examination at the Ni L_{2,3}-edge confirmed the existence of metallic Ni, as its energy loss peak appeared at roughly 860 eV.⁵⁰ These findings suggest that Ni nanoparticles remained virtually unchanged and only work as catalysts during the thermal dehydrogenation of the LiBH₄-2LiNH₂ sample.

3.5. Hydrogenation Properties of the Dehydrogenated Ni@C-Containing Sample. An additional investigation of nanosized Ni@C effects on the hydrogenation performance of the dehydrogenated LiBH₄-2LiNH₂ system was conducted. Two samples of LiBH₄-2LiNH₂ and LiBH₄-2LiNH₂-10 wt % Ni@C were first dehydrogenated to 380 and 350 °C, respectively. The fully dehydrogenated samples were then hydrogenated under 100 bar of hydrogen from room

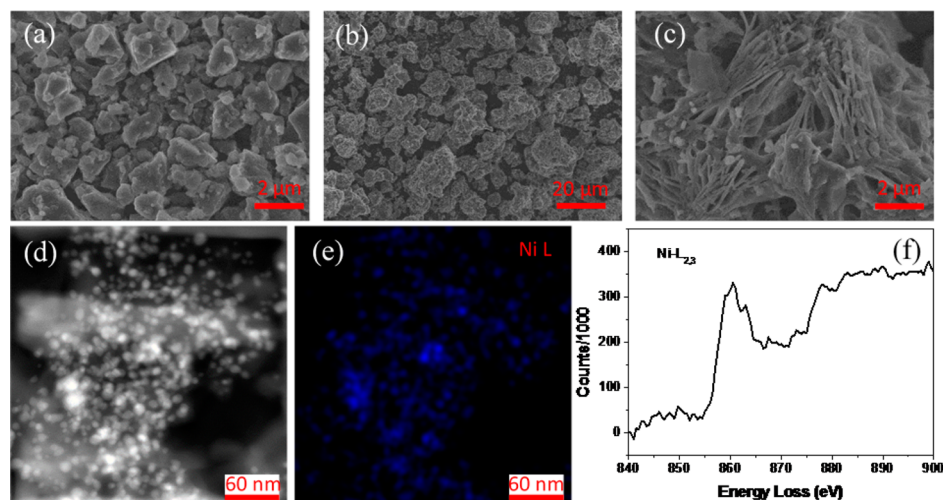


Figure 9. SEM images of the dehydrogenated LiBH₄-2LiNH₂ (a) and LiBH₄-2LiNH₂-10 wt % Ni@C (b,c) samples, the HAADF-STEM image (d), and the corresponding EDS elemental map (e) and EELS spectrum (f) at the Ni L-edge of the dehydrogenated LiBH₄-2LiNH₂-10 wt % Ni@C sample.

temperature to 380 °C. Figure 10(a) presents the hydrogenation curves of the dehydrogenated pristine sample and

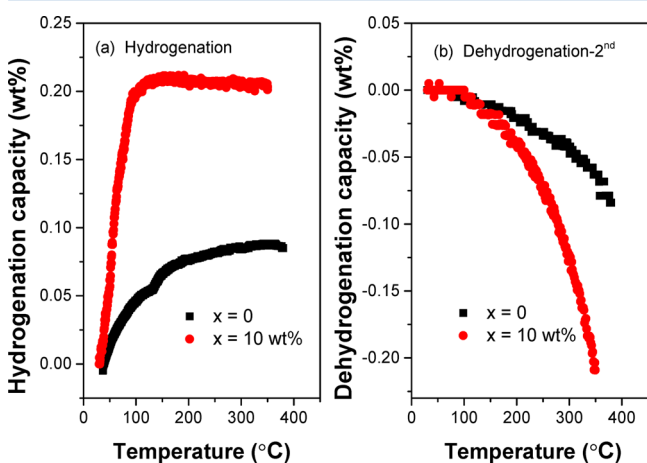


Figure 10. Hydrogenation (a) and rehydrogenation (b) curves of the $\text{LiBH}_4\text{--}2\text{LiNH}_2$ and $\text{LiBH}_4\text{--}2\text{LiNH}_2\text{--}10$ wt % Ni@C samples as a function of temperature.

Ni@C-containing samples as a function of temperature. It was found that only 0.075 wt % of hydrogen was charged into the dehydrogenated pristine sample when heated to 380 °C. Interestingly, the hydrogen uptake level increased to approximately 0.2 wt % for the dehydrogenated nanosized Ni@C-containing sample under identical conditions. The follow-up dehydrogenation experiment further confirmed this improvement as shown in Figure 10(b). These results indicate that the presence of nanosized Ni@C slightly improves hydrogenation properties of the $\text{LiBH}_4\text{--}2\text{LiNH}_2$ system. Additional investigations are in progress in our laboratory to achieve high hydrogen storage reversibility levels in the $\text{LiBH}_4\text{--}2\text{LiNH}_2$ system.

4. CONCLUSION

In this work, metallic Ni nanoparticles supported by carbon (called nanosized Ni@C) were synthesized by calcining FA-filled MOF-74(Ni) at 700 °C. The prepared nanosized Ni@C included 64.2 wt % of Ni and 35.8 wt % of C. It was introduced into the $\text{LiBH}_4\text{--}2\text{LiNH}_2$ system as a catalyst to improve hydrogen storage properties. The results show that the $\text{LiBH}_4\text{--}2\text{LiNH}_2\text{--}10$ wt % Ni@C sample released approximately 10.0 wt % of hydrogen at below 250 °C, constituting a 110 °C reduction in terminal dehydrogenation temperatures relative to those of the pristine sample. In particular, virtually all of the hydrogen in the 10 wt % Ni@C-containing sample was rapidly released within 21 min at 220 °C, while less than 0.5 wt % of hydrogen was released from the pristine $\text{LiBH}_4\text{--}2\text{LiNH}_2$ sample under identical conditions. This dramatically decreased kinetic barrier is responsible for a significant reduction in dehydrogenation operating temperatures. Structural analyses revealed that nanosized metallic Ni remained nearly unchanged and only worked as a catalyst for hydrogen release from the $\text{LiBH}_4\text{--}2\text{LiNH}_2$ system. The dehydrogenated Ni@C-containing sample presented a loose porous morphology and could collect approximately 0.2 wt % of hydrogen under 100 bar of hydrogen, which is superior to the pristine sample. However, further investigations should be conducted to achieve much higher levels of hydrogen storage reversibility in the $\text{LiBH}_4\text{--}2\text{LiNH}_2$ system.

ASSOCIATED CONTENT

Supporting Information

The Supporting Information is available free of charge on the ACS Publications website at DOI: 10.1021/acs.jpcc.5b09256.

XRD patterns of the reported and prepared MOF-74(Ni) and the 500 °C-heated Ni@C sample under air atmosphere (PDF)

AUTHOR INFORMATION

Corresponding Author

*E-mail: mselyf@zju.edu.cn. Tel./Fax: +86 571 87952615.

Notes

The authors declare no competing financial interest.

ACKNOWLEDGMENTS

We gratefully acknowledge financial support received from the National Natural Science Foundation of China (51171170, 51222101), the Research Fund for the Doctoral Program of Higher Education of China (20130101110080, 20130101130007), the Program for Innovative Research Team at the University of Ministry of Education of China (IRT13037), Zhejiang Provincial Natural Science Foundation of China (LR16E010002), and from the Fundamental Research Funds for the Central Universities (2014XZZX003-08, 2014XZZX005).

REFERENCES

- Pellow, M. A.; Emmott, C. J. M.; Barnhart, C. J.; Benson, S. M. Hydrogen or Batteries for Grid Storage? A Net Energy Analysis. *Energy Environ. Sci.* **2015**, 8, 1938–1952.
- Schlappach, L.; Züttel, A. Hydrogen-Storage Materials for Mobile Applications. *Nature* **2001**, 414, 353–358.
- Cipriani, G.; Di Dio, V.; Genduso, F.; La Cascia, D.; Liga, R.; Miceli, R.; Galluzzo, G. R. Perspective on Hydrogen Energy Carrier and Its Automotive Applications. *Int. J. Hydrogen Energy* **2014**, 39, 8482–8494.
- Schüth, F.; Bogdanović, B.; Felderhoff, M. Light Metal Hydrides and Complex Hydrides for Hydrogen Storage. *Chem. Commun.* **2004**, 21, 2249–2258.
- Orimo, S. I.; Nakamori, Y.; Eliseo, J. R.; Züttel, A.; Jensen, C. M. Complex Hydrides for Hydrogen Storage. *Chem. Rev.* **2007**, 107, 4111–4132.
- Jain, I. P.; Jain, P.; Jain, A. Novel Hydrogen Storage Materials: A Review of Lightweight Complex Hydrides. *J. Alloys Compd.* **2010**, 503, 303–339.
- Liang, C.; Liu, Y. F.; Fu, H. L.; Ding, Y. F.; Gao, M. X.; Pan, H. G. Li–Mg–N–H-Based Combination Systems for Hydrogen Storage. *J. Alloys Compd.* **2011**, 509, 7844–7853.
- Li, L.; Xu, C. C.; Chen, C. C.; Wang, Y. J.; Jiao, L. F.; Yuan, H. T. Sodium Alanate System for Efficient Hydrogen Storage. *Int. J. Hydrogen Energy* **2013**, 38, 8798–8812.
- Bogdanović, B.; Schwichardi, M. Ti-Doped Alkali Metal Aluminium Hydrides as Potential Novel Reversible Hydrogen Storage Materials. *J. Alloys Compd.* **1997**, 253, 1–9.
- Züttel, A.; Wenger, P.; Rentsch, S.; Sudan, P.; Mauron, P.; Emmenegger, C. LiBH_4 a New Hydrogen Storage Material. *J. Power Sources* **2003**, 118, 1–7.
- Li, H. W.; Yan, Y. G.; Orimo, S. I.; Züttel, A.; Jensen, C. M. Recent Progress in Metal Borohydrides for Hydrogen Storage. *Energies* **2011**, 4, 185–214.
- Chen, P.; Xiong, Z. T.; Luo, J. Z.; Lin, J. Y.; Tan, K. L. Interaction of Hydrogen with Metal Nitrides and Imides. *Nature* **2002**, 420, 302–304.
- Xiong, Z. T.; Yong, C. K.; Wu, G. T.; Chen, P.; Shaw, W.; Karkamkar, A.; Autrey, T.; Jones, M. O.; Johnson, S. R.; Edwards, P.

- P.; David, W. I. F. High-Capacity Hydrogen Storage in Lithium and Sodium Amidoboranes. *Nat. Mater.* **2008**, *7*, 138–141.
- (14) Soloveichik, G.; Her, J. H.; Stephens, P. W.; Gao, Y.; Rijssenbeek, J.; Andrus, M.; Zhao, J. C. Ammine Magnesium Borohydride Complex as a New Material for Hydrogen Storage: Structure and Properties of $Mg(BH_4)_2 \cdot 2NH_3$. *Inorg. Chem.* **2008**, *47*, 4290–4298.
- (15) Ley, M. B.; Jepsen, L. H.; Lee, Y. S.; Cho, Y. W.; von Colbe, J. M. B.; Dornheim, M.; Rokni, M.; Jensen, J. O.; Sloth, M.; Filinchuk, Y.; Jørgensen, J. E.; Besenbacher, F.; Jensen, T. R. Complex Hydrides for Hydrogen Storage – New Perspectives. *Mater. Today* **2014**, *17*, 122–128.
- (16) Vajo, J. J.; Skeith, S. L.; Mertens, F. Reversible Storage of Hydrogen in Destabilized $LiBH_4$. *J. Phys. Chem. B* **2005**, *109*, 3719–3722.
- (17) Li, W. Y.; Li, C. S.; Ma, H.; Chen, J. Magnesium Nanowires: Enhanced Kinetics for Hydrogen Absorption and Desorption. *J. Am. Chem. Soc.* **2007**, *129*, 6710–6711.
- (18) Liu, Y. F.; Wang, F. H.; Cao, Y. H.; Gao, M. X.; Pan, H. G.; Wang, Q. D. Mechanisms for the Enhanced Hydrogen Desorption Performance of the TiF_4 -catalyzed Na_2LiAlH_6 Used for Hydrogen Storage. *Energy Environ. Sci.* **2010**, *3*, 645–653.
- (19) Li, Y. T.; Fang, F.; Fu, H. L.; Qiu, J. M.; Song, Y.; Li, Y. S.; Sun, D. L.; Zhang, Q. G.; Ouyang, L. Z.; Zhu, M. Carbon Nanomaterial-Assisted Morphological Tuning for Thermodynamic and Kinetic Destabilization in Sodium Alanates. *J. Mater. Chem. A* **2013**, *1*, 5238–5246.
- (20) Cai, W. T.; Wang, H.; Liu, J. W.; Jiao, L. F.; Wang, Y. J.; Ouyang, L. Z.; Sun, T.; Sun, D. L.; Wang, H. H.; Yao, X. D.; Zhu, M. Towards Easy Reversible Dehydrogenation of $LiBH_4$ by Catalyzing Hierarchic Nanostructured CoB. *Nano Energy* **2014**, *10*, 235–244.
- (21) Li, L.; Xu, Y. N.; Wang, Y.; Wang, Y. J.; Qiu, F. Y.; An, C. H.; Jiao, L. F.; Yuan, H. T. NbN Nanoparticles as Additive for the High Dehydrogenation Properties of $LiAlH_4$. *Dalton Trans.* **2014**, *43*, 1806–1813.
- (22) Pang, Y. P.; Liu, Y. F.; Gao, M. X.; Ouyang, L. Z.; Liu, J. W.; Wang, H.; Zhu, M.; Pan, H. G. A Mechanical-Force-Driven Physical Vapour Deposition Approach to Fabricating Complex Hydride Nanostructures. *Nat. Commun.* **2014**, *5*, 1–9.
- (23) Zhang, X.; Liu, Y. F.; Wang, K.; Gao, M. X.; Pan, H. G. Remarkably Improved Hydrogen Storage Properties of Nanocrystalline TiO_2 -Modified $NaAlH_4$ and Evolution of Ti containing Species During Dehydrogenation/Hydrogenation. *Nano Res.* **2015**, *8*, 533–545.
- (24) Yan, Y. G.; Remhof, A.; Rentsch, D.; Züttel, A.; Giri, S.; Jena, P. A Novel Strategy for Reversible Hydrogen Storage in $Ca(BH_4)_2$. *Chem. Commun.* **2015**, *51*, 11008–11011.
- (25) Chen, P.; Xiong, Z. T.; Luo, J. Z.; Lin, J. Y.; Tan, K. L. Interaction between Lithium Amide and Lithium Hydride. *J. Phys. Chem. B* **2003**, *107*, 10967–10970.
- (26) Lu, J.; Fang, Z. G. Z.; Sohn, H. Y. A Dehydrogenation Mechanism of Metal Hydrides Based on Interactions between H^{+} and H^- . *Inorg. Chem.* **2006**, *45*, 8749–8754.
- (27) Pinkerton, F. E.; Meisner, G. P.; Meyer, M. S.; Balogh, M. P.; Kundrat, M. D. Hydrogen Desorption Exceeding Ten Weight Percent from the New Quaternary Hydride $Li_3BN_2H_8$. *J. Phys. Chem. B* **2005**, *109*, 6–8.
- (28) Liu, Y. F.; Hu, J. J.; Wu, G. T.; Xiong, Z. T.; Chen, P. Large Amount of Hydrogen Desorption from the Mixture of $Mg(NH_2)_2$ and $LiAlH_4$. *J. Phys. Chem. C* **2007**, *111*, 19161–19164.
- (29) Chua, Y. S.; Chen, P.; Wu, G. T.; Xiong, Z. T. Development of Amidoboranes for Hydrogen Storage. *Chem. Commun.* **2011**, *47*, 5116–5129.
- (30) Guo, Y. H.; Yu, X. B.; Sun, W. W.; Sun, D. L.; Yang, W. N. The Hydrogen-Enriched Al–B–N System as an Advanced Solid Hydrogen-Storage Candidate. *Angew. Chem., Int. Ed.* **2011**, *50*, 1087–1091.
- (31) Yang, Y. J.; Liu, Y. F.; Li, Y.; Gao, M. X.; Pan, H. G. Synthesis and Thermal Decomposition Behaviors of Magnesium Borohydride Ammoniates with Controllable Composition as Hydrogen Storage Materials. *Chem. - Asian J.* **2013**, *8*, 476–481.
- (32) Yang, Y. J.; Liu, Y. F.; Wu, H.; Zhou, W.; Gao, M. X.; Pan, H. G. An Ammonia-Stabilized Mixed-Cation Borohydride: Synthesis, Structure and Thermal Decomposition Behaviour. *Phys. Chem. Chem. Phys.* **2014**, *16*, 135–143.
- (33) Yang, Y. J.; Liu, Y. F.; Li, L.; Gao, M. X.; Pan, H. G. Heating Rate-Dependent Dehydrogenation in the Thermal Decomposition Process of $Mg(BH_4)_2 \cdot 6NH_3$. *J. Phys. Chem. C* **2013**, *117*, 16326–16335.
- (34) Huang, J. M.; Tan, Y. B.; Su, J. H.; Gu, Q. F.; Černý, R.; Ouyang, L. Z.; Sun, D. L.; Yu, X. B.; Zhu, M. Synthesis, Structure and Dehydrogenation of Zirconium Borohydride Octammoniate. *Chem. Commun.* **2015**, *51*, 2794–2797.
- (35) Paik, B.; Li, H. W.; Wang, J. H.; Akiba, E. A $Li-Mg-N-H$ Composite as H_2 Storage Material: a Case Study with $Mg(NH_2)_2 \cdot 4LiH-LiNH_2$. *Chem. Commun.* **2015**, *51*, 10018–10021.
- (36) Meisner, G. P.; Scullin, M. L.; Balogh, M. P.; Pinkerton, F. E.; Meyer, M. S. Hydrogen Release from Mixtures of Lithium Borohydride and Lithium Amide: a Phase Diagram Study. *J. Phys. Chem. B* **2006**, *110*, 4186–4192.
- (37) Pinkerton, F. E.; Meyer, M. S.; Meisner, G. P.; Balogh, M. P. Improved Hydrogen Release from $LiB_{0.33}N_{0.67}H_{2.67}$ with Noble Metal Additions. *J. Phys. Chem. B* **2006**, *110*, 7967–7974.
- (38) Pinkerton, F. E.; Meyer, M. S.; Meisner, G. P.; Balogh, M. P. Improved Hydrogen Release from $LiB_{0.33}N_{0.67}H_{2.67}$ with Metal Additives: Ni, Fe, and Zn. *J. Alloys Compd.* **2007**, *433*, 282–291.
- (39) Tang, W. S.; Wu, G. T.; Liu, T.; Wee, A. T. S.; Yong, C. K.; Xiong, Z. T.; Hor, A. T. S.; Chen, P. Cobalt-Catalyzed Hydrogen Desorption from the $LiNH_2-LiBH_4$ System. *Dalton Trans.* **2008**, 2395–2399.
- (40) Liu, Y. F.; Luo, K.; Zhou, Y. F.; Gao, M. X.; Pan, H. G. Diffusion Controlled Hydrogen Desorption Reaction for the $LiBH_4/2LiNH_2$ System. *J. Alloys Compd.* **2009**, *481*, 473–479.
- (41) Zhang, Y.; Liu, Y. F.; Pang, Y. P.; Gao, M. X.; Pan, H. G. Role of Co_3O_4 in Improving the Hydrogen Storage Properties of a $LiBH_4-2LiNH_2$ Composite. *J. Mater. Chem. A* **2014**, *2*, 11155–11161.
- (42) Zhang, Y.; Liu, Y. F.; Liu, T.; Gao, M. X.; Pan, H. G. Remarkable Decrease in Dehydrogenation Temperature of $Li-B-N-H$ Hydrogen Storage System with CoO Additive. *Int. J. Hydrogen Energy* **2013**, *38*, 13318–13327.
- (43) Caskey, S. R.; Wong-Foy, A. G.; Matzger, A. J. Dramatic Tuning of Carbon Dioxide Uptake via Metal Substitution in a Coordination Polymer with Cylindrical Pores. *J. Am. Chem. Soc.* **2008**, *130*, 10870–10871.
- (44) Filinchuk, Y. E.; Yvon, K.; Meisner, G. P.; Pinkerton, F. E.; Balogh, M. P. On the Composition and Crystal Structure of the New Quaternary Hydride Phase $Li_4BN_3H_{10}$. *Inorg. Chem.* **2006**, *45*, 1433–1435.
- (45) Chater, P. A.; David, W. I. F.; Anderson, P. A. Synthesis and Structure of the New Complex Hydride $Li_2BH_4NH_2$. *Chem. Commun.* **2007**, *45*, 4770–4772.
- (46) Wu, H.; Zhou, W.; Udoovic, T. J.; Rush, J. J.; Yildirim, T. Structures and Crystal Chemistry of Li_2BNH_6 and $Li_4BN_3H_{10}$. *Chem. Mater.* **2008**, *20*, 1245–1247.
- (47) Kissinger, H. E. Reaction Kinetics in Differential Thermal Analysis. *Anal. Chem.* **1957**, *29*, 1702–1706.
- (48) Pinkerton, F. E.; Meyer, M. S. Hydrogen Desorption Behavior of Nickel-Chloride-Catalyzed Stoichiometric $Li_4BN_3H_{10}$. *J. Phys. Chem. C* **2009**, *113*, 11172–11176.
- (49) Chater, P. A.; David, W. I. F.; Johnson, S. R.; Edwards, P. P.; Anderson, P. A. Synthesis and Crystal Structure of $Li_4BH_4(NH_2)_3$. *Chem. Commun.* **2006**, *23*, 2439–2441.
- (50) Rojas, T. C.; Sayagués, M. J.; Caballero, A.; Koltypin, Y.; Gedanken, A.; Ponsonnet, L.; Vacher, B.; Martin, J. M.; Fernández, A. TEM, EELS and EFTEM Characterization of Nickel Nanoparticles Encapsulated in Carbon. *J. Mater. Chem.* **2000**, *10*, 715–721.